TISSUE ENGINEERING: Part A
Volume 21, Numbers 3 and 4, 2015

DOI: 10.1089/ten.tea.2014.0384

Cartilage Repair and Subchondral Bone Remodeling in Response to Focal Lesions in a Mini-Pig Model: Implications for Tissue Engineering

Matthew B. Fisher, PhD,[1,2] Nicole S. Belkin, MD,[1,2] Andrew H. Milby, MD,[1,2] Elizabeth A. Henning, BS,[1,2] Marc Bostrom, MS,[1,2] Minwook Kim, MS,[1,2] Christian Pfeifer, MD,[1,2] Gregory Meloni, MS,[1,2] George R. Dodge, PhD,[1,2] Jason A. Burdick, PhD,[2,3] Thomas P. Schaer, VMD,[4] David R. Steinberg, MD,[1,2] and Robert L. Mauck, PhD[1–3]

Objective: Preclinical large animal models are essential for evaluating new tissue engineering (TE) technologies and refining surgical approaches for cartilage repair. Some preclinical animal studies, including the commonly used minipig model, have noted marked remodeling of the subchondral bone. However, the mechanisms underlying this response have not been well characterized. Thus, our objective was to compare *in-vivo* outcomes of chondral defects with varied injury depths and treatments.
Design: Trochlear chondral defects were created in 11 Yucatan minipigs (6 months old). Groups included an untreated partial-thickness defect (PTD), an untreated full-thickness defect (FTD), and FTDs treated with microfracture, autologous cartilage transfer (FTD-ACT), or an acellular hyaluronic acid hydrogel. Six weeks after surgery, micro-computed tomography (μCT) was used to quantitatively assess defect fill and subchondral bone remodeling. The quality of cartilage repair was assessed using the ICRS-II histological scoring system and immunohistochemistry for type II collagen. A finite element model (FEM) was developed to assess load transmission.
Results: Using μCT, substantial bone remodeling was observed for all FTDs, but not for the PTD group. The best overall histological scores and greatest type II collagen staining was found for the FTD-ACT and PTD groups. The FEM confirmed that only the FTD-ACT group could initially restore appropriate transfer of compressive loads to the underlying bone.
Conclusions: The bony remodeling observed in this model system appears to be a biological phenomena and not a result of altered mechanical loading, with the depth of the focal chondral defect (partial vs. full thickness) dictating the bony remodeling response. The type of cartilage injury should be carefully controlled in studies utilizing this model to evaluate TE approaches for cartilage repair.

Introduction

Damage to articular cartilage evokes a limited healing response and frequently progresses to joint-wide osteoarthritis (OA). Focal cartilage defects occur due to sports, trauma, or other activities of daily living, and the majority of these injuries involve a compromised articular layer, but do not extend into the subchondral bone.[1,2] However, these focal cartilage defects can impair quality of life to the same extent as more widespread OA changes in the joint.[3] Furthermore, such injuries can also engender stress concentrations at the defect boundaries, predisposing the adjacent cartilage to progressive degeneration.[4,5] As such, there is substantial interest in treating localized defects in young and/or active patient populations.[6,7]

A variety of options have emerged for treating focal cartilage defects, including microfracture, allogeneic or autologous osteochondral grafting, autologous chondrocyte implantation (ACI), and matrix-induced ACI.[6,8–12] While not yet in clinical practice, many other tissue engineering (TE) and regenerative medicine approaches have also been pursued with some approaches achieving biomechanical and biochemical properties on the order of native cartilage.[13–22]

When translating new TE technologies and surgical approaches to preclinical large animal models, it is important to note that the type of defect can vary substantially (e.g.,

[1]McKay Orthopaedic Research Laboratory, Department of Orthopaedic Surgery, Perelman School of Medicine, University of Pennsylvania, Philadelphia, Pennsylvania.
[2]Translational Musculoskeletal Research Center, Philadelphia VA Medical Center, Philadelphia, Pennsylvania.
[3]Department of Bioengineering, University of Pennsylvania, Philadelphia, Pennsylvania.
[4]Comparative Orthopedic Research Laboratory, School of Veterinary Medicine, University of Pennsylvania, Kennett Square, Pennsylvania.

partial-thickness chondral vs. full-thickness chondral vs. osteochondral).[23–29] Although full-thickness chondral defects are clinically relevant, the thin cartilage in most species (< 1 mm) raises questions regarding the ability of an implanted construct to remain within the defect postoperatively.[24] One commonly used model, the immature Yucatan minipig, may be advantageous for short-term or proof-of-concept studies given that its relatively thick cartilage (1–2 mm) could allow stable implantation without the need of additional suturing or covering. In addition, the large size of the joints allows creation of multiple defects.

However, several have noted marked remodeling of the subchondral bone after the creation of a purely chondral defect in this immature porcine model.[30–32] Such changes in the subchondral bone may alter how physical signals are transmitted through the implant and complicate interpretation of findings, even though they are likely a part of the natural healing process. Furthermore, the mechanisms underlying this response have not been well characterized.[33] One hypothesis is that the surgical procedure itself creates microscopic damage to the calcified or calcifying cartilage and/or underlying bone, instigating a remodeling response. Alternatively, the lack of mechanical function (i.e., load transmission through the repair tissue or implant material) could lead to subchondral remodeling due to decreased mechanical signaling to the bone.

In this study, we sought to clarify which of these two hypotheses was correct with regard to subchondral remodeling as well as to evaluate the healing of focal cartilage defects (without macroscopic removal of the underlying bone) without treatment and with microfracture, cartilage autograft transfer, and a common TE base material (hyaluronic acid [HA]) in this juvenile Yucatan minipig model. Microfracture is a common clinical intervention that enables us to compare the results in this model to those in the literature. Cartilage autograft transfer represents an ''idealized'' mature TE graft and was implemented in order to test the ability of this model to retain TE constructs within the defect. Together, these experimental groups enabled us to compare cartilage injury configurations that do and do not create microdamage to the subchondral bone (partial- and full-thickness chondral defects) as well as those which do or do not allow for immediate reconstitution of load transfer.

Materials and Methods

All animal procedures were performed at the Philadelphia VA Medical Center with approval from the Institutional Animal Care and Use Committee and in accordance with policies set forth by the National Institutes of Health. Eleven adolescent, male Yucatan minipigs were utilized (Sinclair Bioresources). The animals were sedated with ketamine and xylazine, with anesthesia maintained throughout surgery via isoflurane. Using sterile technique, a medial parapatellar skin incision was made to the stifle joint, followed by a lateral parapatellar arthrotomy. The patella was retracted medially, and chondral defects (4 mm diameter) were created bilaterally in the trochlear groove (four defects per joint) (Fig. 1A). A biopsy punch was used to outline the defect area. To create full-thickness defects (FTDs), a scalpel blade was used to crosshatch the cartilage, and a blunt probe was placed at the edge of the defect and twisted to remove the cartilage. To create partial-thickness defects (PTDs), a curette was used to remove ~50% of the cartilage thickness without violating the subchondral bone.

Experimental groups included (1) an untreated full-thickness defect (FTD-U, $n = 15$); (2) a full-thickness defect treated with an acellular HA hydrogel (FTD-HA) ($n = 10$); (3) a full-thickness defect treated with microfracture (FTD-MF) ($n = 9$); (4) a full-thickness defect treated with autologous cartilage transfer (FTD-ACT) ($n = 7$); and (5) an untreated partial-thickness defect (PTD-U, $n = 5$). For microfracture, three holes with a depth of 2 mm were created and evenly spaced in the defect using an awl. For ACT, an osteochondral sample was taken from the proximal lateral portion of the trochlear groove. A portion of cartilage was isolated to match the depth of the recipient defect. Normal cartilage served as a control for all groups ($n = 18$). Other groups not reported here were also evaluated, giving rise to the unequal sample sizes. In addition, not all groups were performed in the same set of animals.

To form the HA hydrogel, methacrylated HA (MeHA) was synthesized by reacting methacrylic anhydride (Sigma) and 74 kDa HA (Lifecore).[19–21] Two days before surgery, MeHA macromer was sterilized by exposure to a biocidal UV lamp for 15 min and dissolved in saline at 1% (mass/volume) with 0.05% Irgacure-2959 photoinitiator (Ciba-Geigy). Hydrogels were polymerized within the defects via exposure to UV light (365 nm) for 10 min at an intensity of 1 mW/cm^2 (Omnicure S2000; Lumen Dynamics Group).

After defect creation and repair, incisions were closed in layers using absorbable sutures. Animals were provided buprenorphine and carprofen for postoperative pain control. Movement and weight bearing were allowed as tolerated. At 6 weeks postsurgery, all animals were euthanized with an overdose of pentobarbital, and hind limbs were disarticulated at the hip. The trochlear groove of each joint was carefully exposed. After gross inspection, individual cartilage defects with underlying bone as well as normal osteochondral samples were isolated and fixed in 4% paraformaldehyde.

To assess the three-dimensional morphometry of the healing cartilage and bone, micro-computed tomography (μCT) was performed (Viva CT75; Scanco).[34–36] Specimens were first scanned to image the bone (70 kVp, 110 μA). Samples were then placed in an iodine-based contrast solution (Lugol's solution; Sigma) for 48 h and rescanned using the same parameters to visualize the cartilage. Bone volume per total volume (BV/TV) was calculated for the first 2 mm and for a region 3–5 mm beneath the original defect for each specimen. Degree of defect fill was determined as a percentage of the total defect volume from contrast-enhanced μCT images.

After μCT, samples were decalcified (Formical 2000; Decal Chemical Corporation) for 1 week. Samples were then dehydrated, paraffin embedded, sectioned to 6 μm, and stained to assess cell morphology (hematoxylin and eosin) and matrix content (proteoglycan and collagen/fibrous matrix via Safranin O and fast green, respectively). Slides were scored using a modified ICRS-II system[37] by five blinded reviewers, and scores were averaged across reviewers. Immunohistochemistry was performed to assess the deposition of type II collagen. Sections were deparaffinized, rehydrated, and subjected to proteinase K antigen retrieval. Sections were incubated with a type II collagen antibody (5 μg/mL; Developmental Studies Hybridoma Bank, University of Iowa) for 1 h. After washing, the signal was detected using the Millipore Immunoperoxidase

Secondary Detection System (EMD Millipore Corporation). For quantification (ImageJ, National Institutes of Health), images were converted to grayscale, and the area of the defect was outlined. After thresholding, the amount of positive staining was computed as the number of black (positive) pixels divided by the total number of pixels in the defect.

To estimate the initial amount of load transferred to the bone in each experimental scenario, a finite element model (FEM) was constructed. An axisymmetric wedge (5°) representing the cartilage, bone, and filled defect was created in SolidWorks (Dassault Systèmes SolidWorks). The cross-section of both the bone and cartilage was rectangular (10 mm in width and 5 and 1.5 mm in height, respectively). For the PTD-U group, an area of 2 mm in width and 0.75 mm in height was removed from the central portion of the cartilage (Supplementary Fig. S3; Supplementary Data are available online at www.liebertpub.com/tea). Similarly, for the FTD-U group, an area that was 2 mm in width and 1.5 mm in height was removed. To simulate the FTD-HA and FTD-ACT groups, the defect was filled with a separate object that was 2 mm in height and 1.5 mm in width (Supplementary Fig. S3). For each condition, the mesh was generated using commercial software and hexahedral elements (Trelis, v14.0; Computational Simulation Software) and refined near the defect boundary.

FEBio was used to import the mesh, set up and solve the model, and visualize results (© Maas and Weiss).[38] The bone was modeled as a linearly isotropic elastic solid ($E = 150$ MPa, $\nu = 0.3$). The cartilage, cartilage implant, and HA implant were modeled as biphasic materials. The solid matrix of cartilage (0.2 volume fraction) was described as a mixed solid containing a neo-Hookean bulk matrix ($E = 0.56$ MPa, $\nu = 0.28$) and three fiber families orthogonal to each other and along the principal geometric axes of the cartilage with a constitutive equation represented by a power function (modulus of 25 MPa, power of 2).[39,40] The permeability of the cartilage was set to 0.002 $mm^4/N*s$. For the HA hydrogel, the solid matrix (0.01 volume fraction) was described as a neo-Hookean solid ($E = 0.0035$ MPa, $\nu = 0.3$), and the permeability was set to 1.8 $mm^4/N*s$.[41] The fluid pressure at the top surface of the cartilage was set to zero. Nonsliding contact between the cartilage (and implant) and bone was enforced. Between the implant and cartilage, sliding contact allowing fluid flow across the boundary was enforced.

To simulate loading, a 10% compressive strain was applied to the top surface of the cartilage (and implants) over a 1 s period. Maps of the axial stress were created and compared between groups, and the axial stress within bone elements was plotted as a function of distance from the cartilage. Data were collected from bone underneath the defect as well as 2 mm from the defect (underneath normal cartilage).

Statistical analyses were performed using SPSS (version 21; IBM). Normality of each dataset was assessed using the Kolmogorov–Smirnoff test. For μCT on BV/TV data were normally distributed, and so a two-way analysis of variance (ANOVA) was performed with group and zone as independent factors and significance set at $p < 0.05$. Since the datasets had equal variances, a Bonferroni *post-hoc* test was used to assess differences between groups. For defect fill, data were not normally distributed, so the Kruskal–Wallis test was used, followed by individual Mann–Whitney tests between groups. To control for type I error, a Bonferroni correction for multiple comparisons was used ($p < 0.003$). For histological scores, some datasets were normally distributed, while others were not. For normally distributed

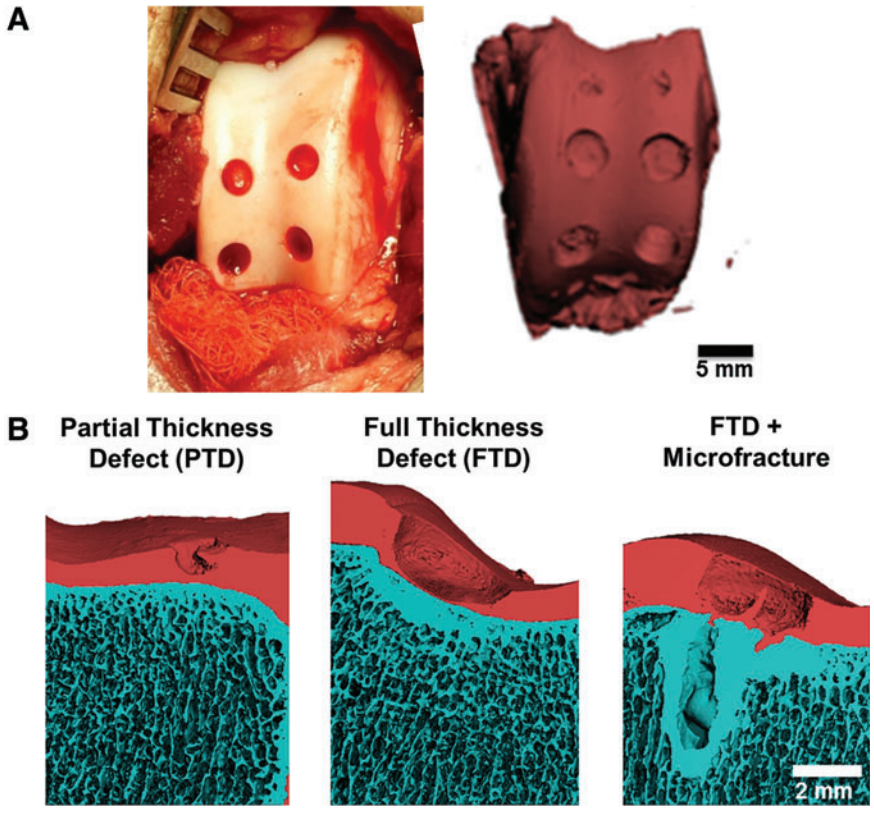

FIG. 1. **(A)** Surgical approach showing location of cartilage defects in the trochlear groove and μCT reconstructions of the entire groove at the time of surgery (scale bar = 5 mm). **(B)** μCT reconstructions of the various injury types at the time of surgery (scale bar = 2 mm). μCT, micro-computed tomography. Color images available online at www.liebertpub.com/tea

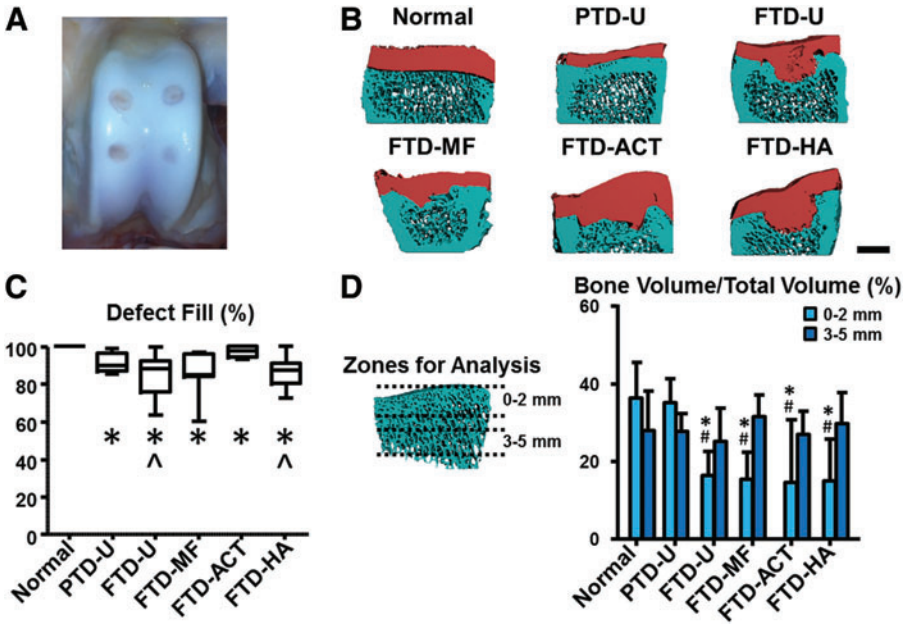

FIG. 2. **(A)** Gross image of a typical trochlear groove after 6 weeks of healing. **(B)** μCT reconstructions of the cross-section of the defect site for different experimental groups (scale bar = 2 mm). **(C)** Quantification of defect fill via μCT. **(D)** Quantification of bone volume per total volume in regions 0–2 and 3–5 mm beneath the original bone/cartilage interface at the center of the injury site ($*p < 0.05$ vs. normal, $^{\#}p < 0.05$ vs. PTD-U, and $\wedge p < 0.05$ vs. FTD-ACT). ACT, autologous cartilage transfer; FTD, full-thickness defect; HA, hyaluronic acid; MF, microfracture; PTD, partial-thickness defect; U, untreated. Color images available online at www.liebertpub.com/tea

data, a one-way ANOVA was performed with Bonferroni or Games–Howell *post-hoc* tests ($p < 0.05$), depending on whether or not the variances were equal between groups. For non-normal data, analyses followed that for the defect fill.

Results

All animals were mobile the day after surgery, had no noticeable gait deficits by 1 week, and completed the study as planned. At the time of surgery, no bleeding was observed when creating the PTDs, while a small amount of bleeding from the subchondral bone was noted after the creation of FTDs (Fig. 1A). However, μCT imaging revealed intact morphology of the subchondral bone plate when FTDs were created (Fig. 1B). Microfracture of the subchondral bone led to greater amounts of blood in the defects and local voids in the subchondral bone (Fig. 1B). At the time of surgery, the autologous cartilage

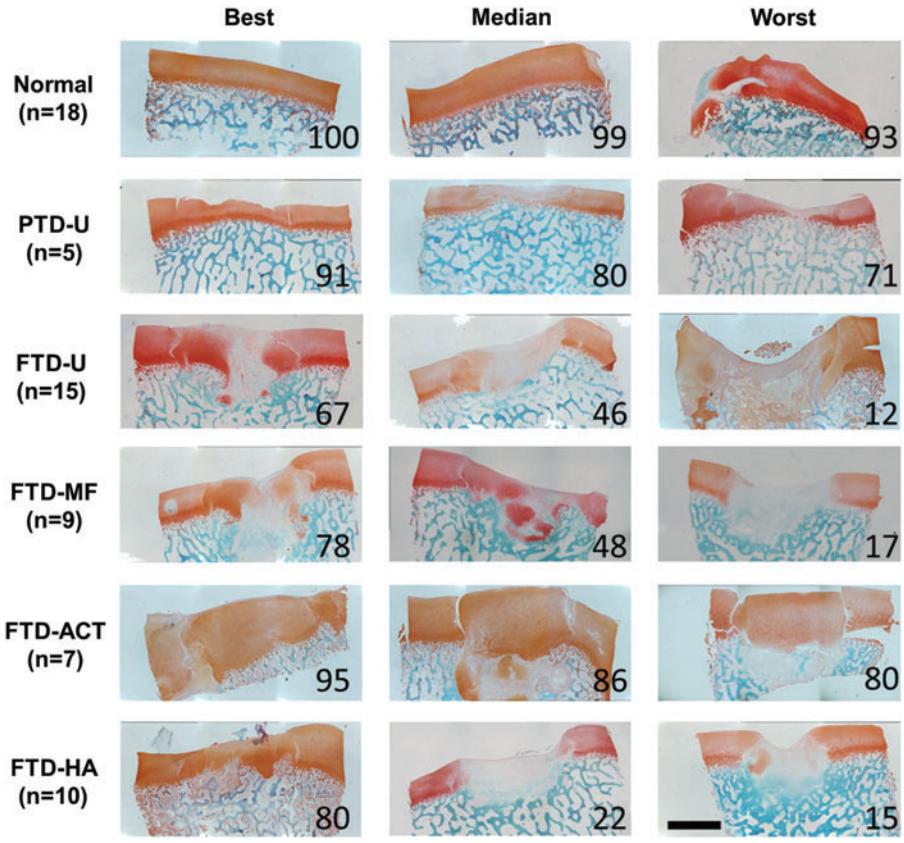

FIG. 3. Histological evaluation of partial- or full-thickness cartilage defects and treatment with microfracture, replacement with articular cartilage, or treatment with an HA hydrogel. Staining (Safranin O/fast green) for proteoglycans (*red*) and proteins (*green*) showing entire defect and adjacent normal tissue. Numbers represent overall histological score for that specimen from ICRS-II scoring (scale bar = 2 mm). Color images available online at www.liebertpub.com/tea

plugs filled the defect and were congruent with the adjacent cartilage. The HA hydrogel gelled within and filled the defect.

Six weeks after surgery (Fig. 2A, B), partial-thickness defects (PTD-U) remained unfilled, although some new tissue was observed on the surface. The untreated full thickness (FTD-U), microfracture-treated (FTD-MF), and HA-treated (FTD-HA) defects were filled with a fibrous tissue that did not completely fill the defect. Interestingly, the HA hydrogel was not readily observed within the defect and was replaced by new tissue. The ACT plugs were still clearly observed in the defects and remained relatively flush with the surrounding cartilage (FTD-ACT). These results were verified by μCT (Fig. 2C). Relative to normal (100% defect fill), all treatment groups had significantly lower defect fill, with median values ranging from 85% in the FTD-MF group to 98% in the FTD-ACT group ($p < 0.003$). The FTD-ACT group provided a significantly higher defect fill relative to the FTD-U and FTD-HA groups ($p < 0.003$).

PTDs showed little to no bone remodeling, while defects through the full cartilage thickness showed clear evidence of remodeling and resorption beneath the defects, with regional differences (Fig. 2B). Quantitatively, within 2 mm of the original cartilage/bone interface, the BV/TV for the PTD-U group was similar to normal (Fig. 2D, $p > 0.05$). However, values for all FTD groups ranged between 55% and 60% lower than normal ($p < 0.05$). In addition, the FTD groups were 53–58% lower than the PTD-U group ($p < 0.05$). However, in the region deeper (3–5 mm) from the original cartilage/bone interface, no differences were found between any treatment groups and control specimens ($p > 0.05$).

Proteoglycan and fibrous tissue deposition in the repair was assessed via Safranin O/Fast Green staining (Figs. 3 and 4), and cellular morphology was assessed via hematoxylin and eosin staining (Fig. 5 and Supplementary Fig. S1). PTD-U specimens had positive staining for proteoglycans and round chondrocyte-like cells. An irregular surface remained, and, in some cases, a new, fibrous lining was observed, featuring elongated cells. The FTD-U group was filled incompletely with a fibrocartilaginous or mostly fibrous tissue, with cell morphology ranging from rounded cells to more elongated ones. MF treatment led to a similar appearance, with some samples showing more robust staining for proteoglycans and chondrocyte-like cells. ACT treatment resulted in tissue that filled the vast majority of the defect space and stained well for proteoglycans and chondrocyte-like cells; however, these constructs were quite variable in their integration with the surrounding tissue. HA treatment appeared similar in terms of matrix and cellular composition to the FTD-U and FTD-MF groups.

Histologic observations were quantified via the ICRS-II scoring system (Fig. 6 and Supplementary Fig. S2). A consistent pattern emerged for most subcategories, where the PTD-U and FTD-ACT groups had the highest median scores with the lowest variability. For some measures, MF showed a slight improvement in median score relative to untreated controls (e.g., Surface Assessment and Defect Fill); however, this change was minor relative to the variability observed. Filling the defect with an HA hydrogel had little impact on the scores relative to untreated controls. Using the overall scores as an example, the average values for the FTD groups were 12–67% lower than normal ($p < 0.05$), while the PTD-U group was similar to normal ($p > 0.05$). In addition, scores for the FTD-U group were 46% and 49% lower than the untreated PTD-U and FTD-ACT groups, respectively ($p < 0.05$). The

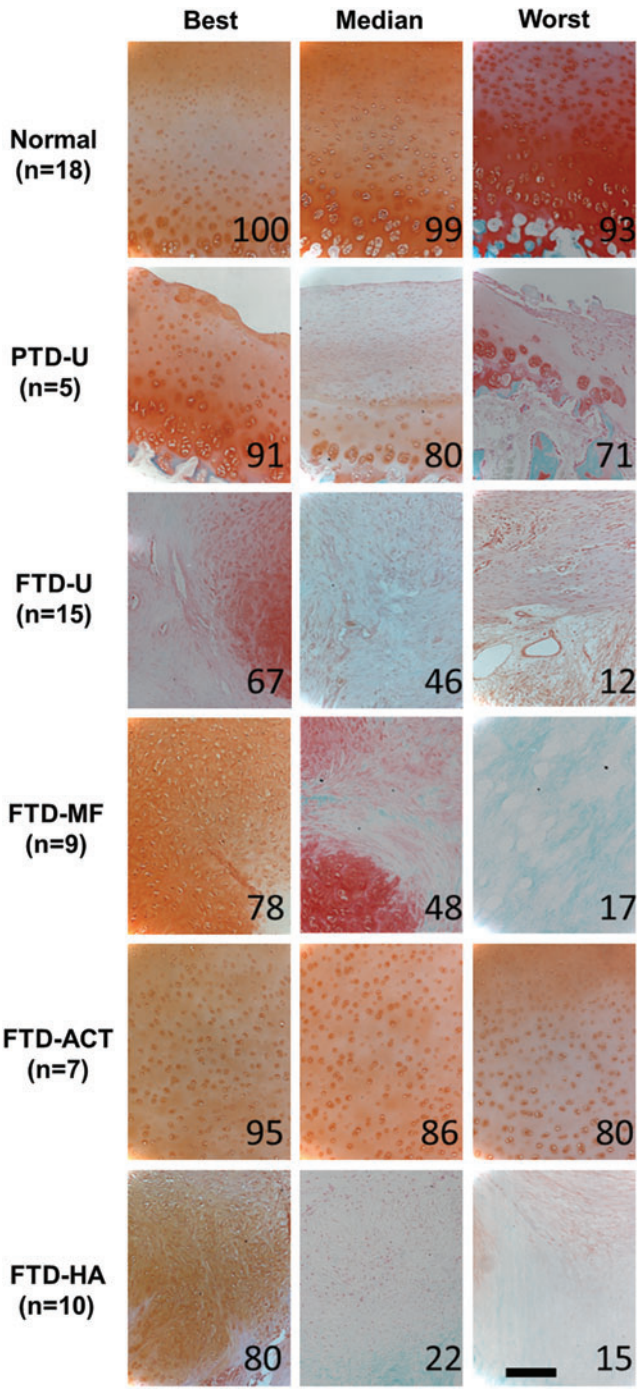

FIG. 4. Higher magnification images of neo-tissue in defect for partial- or full-thickness cartilage defects and treatment with microfracture, replacement with articular cartilage, or treatment with an HA hydrogel. Staining (Safranin O/fast green) for proteoglycans (*red*) and proteins (*green*). Numbers represent overall histological score for that specimen from ICRS-II scoring (scale bar = 200 μm). Color images available online at www.liebertpub.com/tea

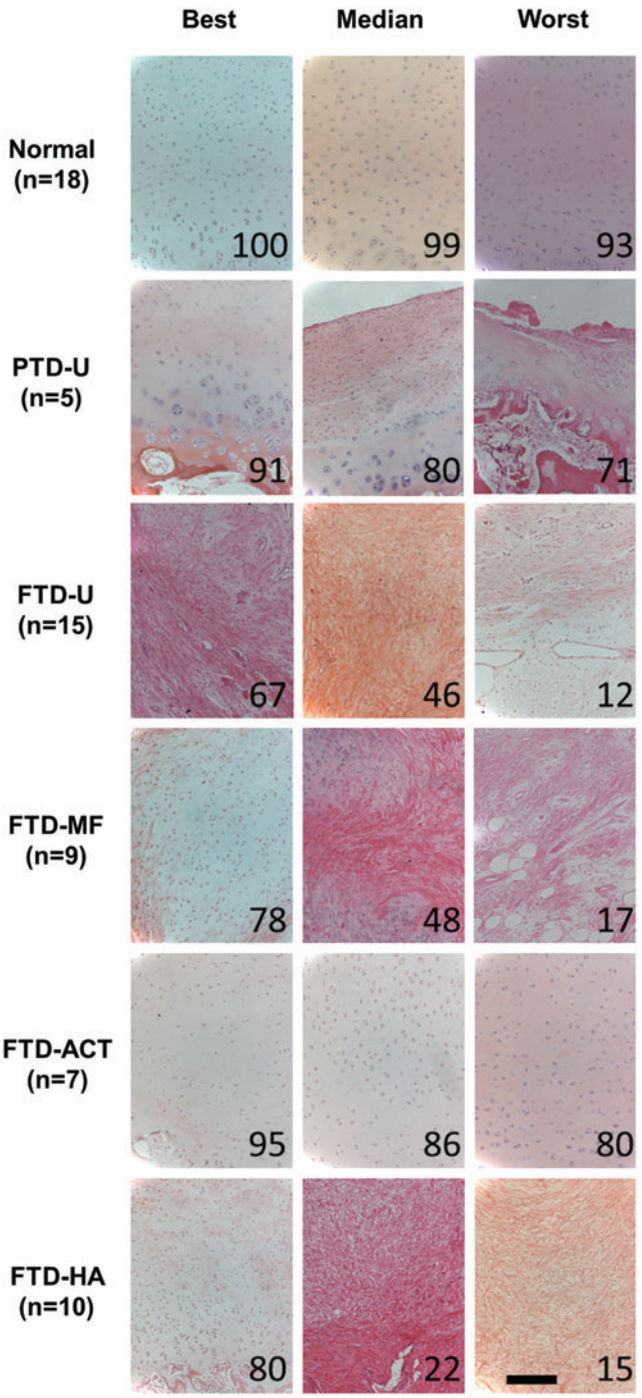

FIG. 5. Staining (hematoxylin and eosin) for cells and matrix within neo-tissue in defect for partial- or full-thickness cartilage defects and treatment with microfracture, replacement with articular cartilage, or treatment with an HA hydrogel. Numbers represent overall histological score for that specimen from ICRS-II scoring (scale bar = 200 μm). Color images available online at www.liebertpub.com/tea

FTD-MF and FTD-HA groups had similar values and were significantly lower than the untreated PTD-U and FTD-ACT groups ($p < 0.05$). Individual scoring of the surface and deep zones as well as other categories, such as matrix staining and cellular morphology, followed a similar trend.

A few exceptions emerged. In the scoring of lateral integration, all experimental groups were significantly lower than normal controls ($p < 0.05$), and here, the FTD-ACT group had the lowest median scores with the greatest range in scores. For bone remodeling, the trends followed those derived from μCT. PTD-U specimens were similar to normal ($p > 0.05$), while all full-thickness groups were significantly lower than normal ($p < 0.05$), with the FTD-ACT group as the lone exception ($p > 0.05$). Moreover, the FTD-U, FTD-MF, and FTD-HA groups were 33%, 44%, and 30% lower than the PTD-U group, respectively ($p < 0.05$). For completeness, other categories, such as cell clustering at the surface, surface architecture, basal integration, vascularization, and tidemark formation, are presented in Supplementary Figure S2.

Type II collagen deposition within the defect was assessed via immunohistochemistry (Fig. 7), and the trends followed those for the general matrix staining in Figure 4. Quantification of type II collagen staining showed abundant and consistent levels in the PTD-U group (81% ± 14%) and the FTD-ACT group (92% ± 5%), similar to normal (96% ± 3%, $p > 0.05$). Variable levels of staining were observed in the FTD-U (44% ± 22%), FTD-MF (51% ± 34%), and FTD-HA defects (27% ± 17%), with some samples showing areas of positive staining, while others showed none. All three groups were significantly lower compared to the normal tissue and the FTD-ACT group ($p < 0.05$). In addition, the FTD-U and FTD-HA groups were 46% and 66% lower, respectively, than the PTD-U group ($p < 0.05$).

As a final consideration of the initial load distribution to the bone in the various groups, we developed a simple FE model of the experimental conditions (Supplementary Fig. S3). When the cartilage was compressed, the bone underneath both the PTD-U and FTD-U defects carried very little stress at a location that was 0.5 mm from the cartilage/bone interface, an order of magnitude lower relative to the bone underneath the surrounding normal cartilage (Fig. 8A). There was a depth-dependent response, as the stress in the bone increased by 1.5–1.7 MPa as the distance from the cartilage/bone interface increased from 0.5 to 5 mm (Fig. 8B). Filling the defect with a HA hydrogel had little impact on the transfer of stress to the underlying bone. However, implantation of the autologous cartilage plug largely restored the stresses within the bone to levels approaching those underneath normal cartilage (Fig. 8B).

Discussion

In this study, we developed a focal cartilage defect model in the trochlear groove of the immature Yucatan minipig and quantitatively assessed the impact of defect severity and subsequent treatment on the cartilage healing response and the degree of remodeling of the subchondral bone. Interestingly, substantial bone remodeling occurred when a FTD was created, but not when a partial-thickness chondral defect was made. The results suggest that the bony remodeling observed in this model system is a biological phenomenon resulting from the injury to the cartilage/bone interface and was not due to altered mechanical loading. Indeed, a simple FE model confirmed that filling the defect with an autologous cartilage plug should enable the initial transfer of compressive loads. Conversely, when left untreated or filled

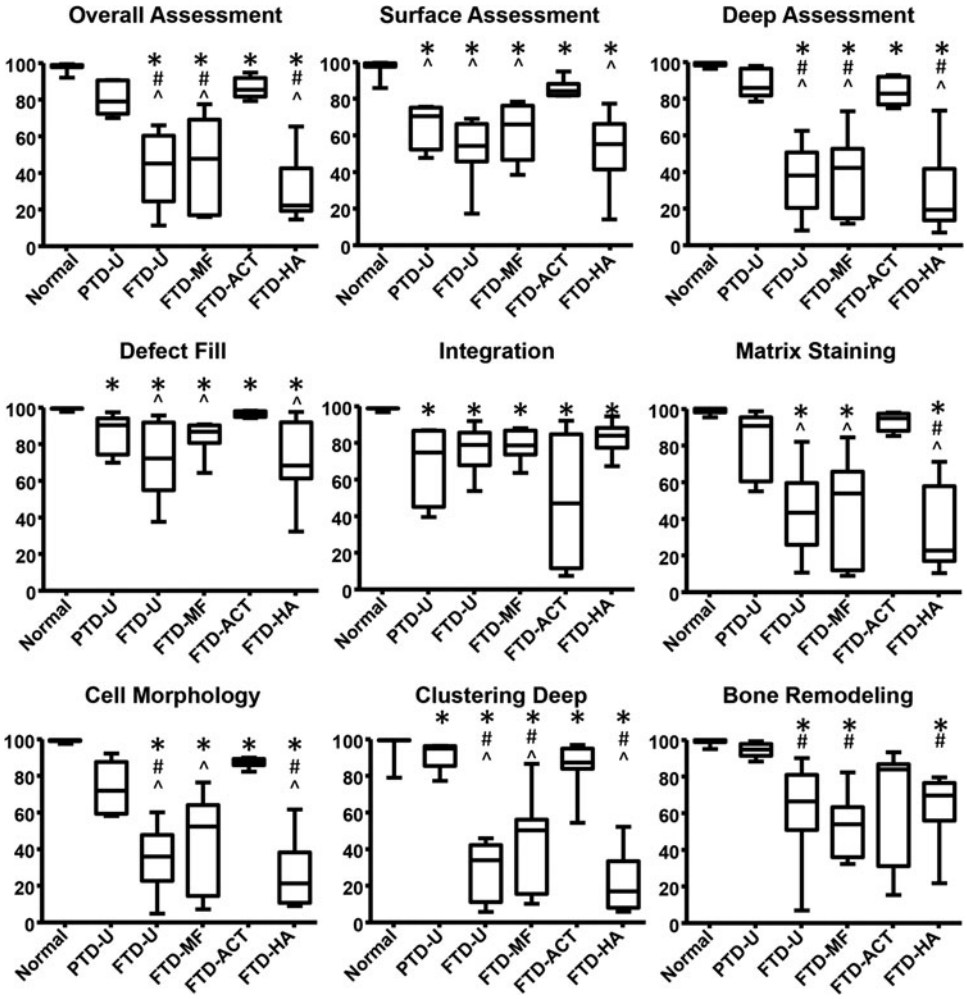

FIG. 6. Histological scoring for all treatment groups based on the ICRS-II scoring system (100 = best, 0 = worst, $^{*}p < 0.05$ vs. normal, $^{\#}p < 0.05$ vs. PTD-U, and $^{\wedge}p < 0.05$ vs. FTD-ACT).

with an HA hydrogel of low compressive modulus, the subchondral bone was predicted to bear little compressive stress initially. Despite this prediction from a simple FE model, a similar remodeling response was observed in all FTD groups, including the ACT group. Moreover, this simple FE model predicted that creation of a partial chondral injury would reduce the initial mechanical load transfer through the cartilage similar to an FTD, and yet, no bony remodeling was found beneath these injuries. Taken together, these results suggest that alterations in mechanical loading were not primarily responsible for the remodeling response seen at this early time point.

Several other studies utilizing immature minipigs have noted this subchondral remodeling response through gross or histological observation.[30–32] One possible reason for this substantial remodeling is the use of an adolescent porcine model, which lacks a well-developed layer of calcified cartilage. Creation of the FTD may have resulted in unavoidable microscopic damage to the forming cartilage/bone interface. While μCT did not show any immediate changes in subchondral bone patency with the creation of FTDs, punctate bleeding within the defect was observed.[5] Animals that have more fully developed layers of calcified cartilage may allow the creation of FTDs without such bony remodeling. For example, studies involving older minipigs (18–24 months) generally do not comment on such a response, and it is not commonly observed histologically.[26,42,43] However, Vasara *et al.* found bony remodeling in a skeletally mature goat model after creation of full-thickness chondral defects.[33] It is still unclear how closely these subchondral changes mimic the human condition, and this is an active area of research.[44] In addition, the time point for evaluation may be critical, as studies have noted early remodeling (< 3 months), but a new bony structure by 12 months.[30,34] Thus, multiple factors (age, species, location of injury, time point for evaluation, etc.) likely impact the presence and degree of the subchondral remodeling response. Nevertheless, even if such events are a part of the natural healing response, it may not be an ideal context in which to evaluate TE cartilage constructs, as they may tend to ''sink'' into the softer remodeling bone beneath the original defect site. Such subsidence would also reduce mechanical load transfer to the implant, potentially altering its growth trajectory after implantation.

Within the cartilage defect itself, the results obtained were consistent with clinical and preclinical studies.[2,6,8–12,26,27,45–49] Without violation of the subchondral bone, cartilage defects have a limited potential to heal with new tissue formation,[2,49] as could be observed for the PTDs in this study. Microfracture of the underlying bone is commonly performed clinically to encourage marrow into the defect, creating a soft immature clot. Although the clot integrates well to the surrounding cartilage, it remodels into a fibrocartilaginous

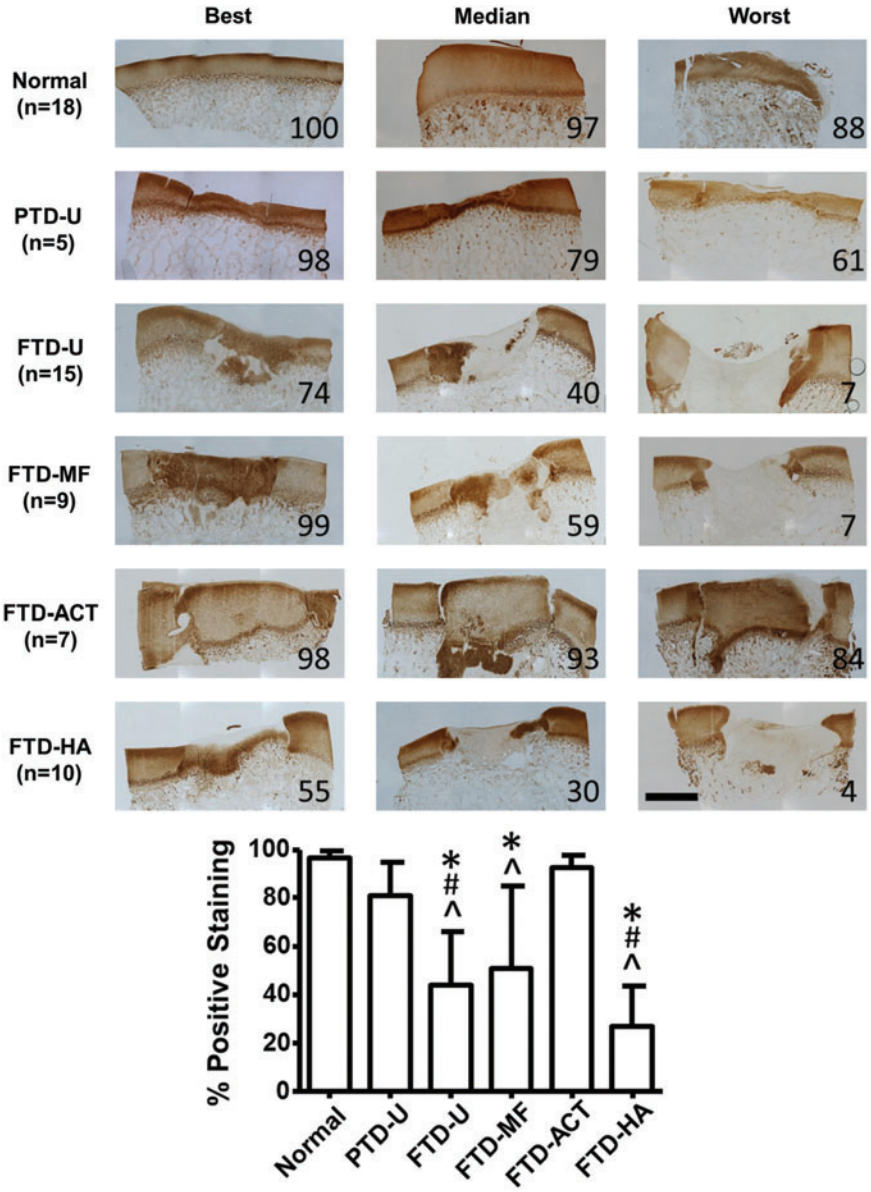

FIG. 7. Immunostaining for collagen type II showing entire defect and adjacent normal tissue for partial- or full-thickness cartilage defects and treatment with microfracture, replacement with articular cartilage, or treatment with an HA hydrogel. Numbers within images and the graph at the bottom indicate the percentage of positive staining within the defect (scale bar = 2 mm, 100 = best, 0 = worst, $*p < 0.05$ vs. normal, $^{\#}p < 0.05$ vs. PTD-U, and $\wedge p < 0.05$ vs. FTD-ACT). Color images available online at www.liebertpub.com/tea

tissue and does not reach native levels of maturity.[8,9,50] In this study, MF treatment, as well as untreated FTDs, led to the formation of a primarily fibrous tissue, with occasional pockets of tissue with a cartilage-like appearance. On the other hand, allogeneic or autologous osteochondral grafts comprising mature native tissue are also clinically used to fill larger defects. Indeed, in this study, transfer of autologous cartilage to the defect was able to restore the histological appearance of the native cartilage, with scores substantially higher than the untreated or MF groups at this early time point. However, the integration of these autologous plugs to the surrounding cartilage was poor, consistent with human clinical and *in-vivo* animal studies.[10,11,46–48] The long-term impact on the loss of mechanical integrity at this interface and the ability of fluid to penetrate into the underlying bone is an area of ongoing research.[51]

Finally, we included an experimental TE group in this study, in which we filled the defect with an HA hydrogel. This is a base material that our group and others has used as a cell-delivery vehicle and scaffold for cartilage TE.[14,19–21] It is important to note that the bioactivity of the HA hydrogel had no discernable impact on bony remodeling or the morphology of the tissue which formed in the cartilage defect. These results are similar to the *in-vivo* findings for other ''scaffold-only'' formulations in the literature.[52,53] This suggests that the presence of an exogenous cell source or chemical factors delivered from these hydrogels will be needed to promote chondrogenesis and cartilage formation.[54] Still, the lack of adverse effects illustrates the biocompatibility of HA-based materials within this injury model.

Collectively, these data provide quantitative outcomes for cartilage repair in a Yucatan minipig trochlear groove cartilage defect model and indicate that the type of cartilage injury should be carefully controlled in future studies to evaluate TE or regenerative medicine approaches. Given the short-term nature of the current work, longer-term studies are also warranted to determine whether the subchondral

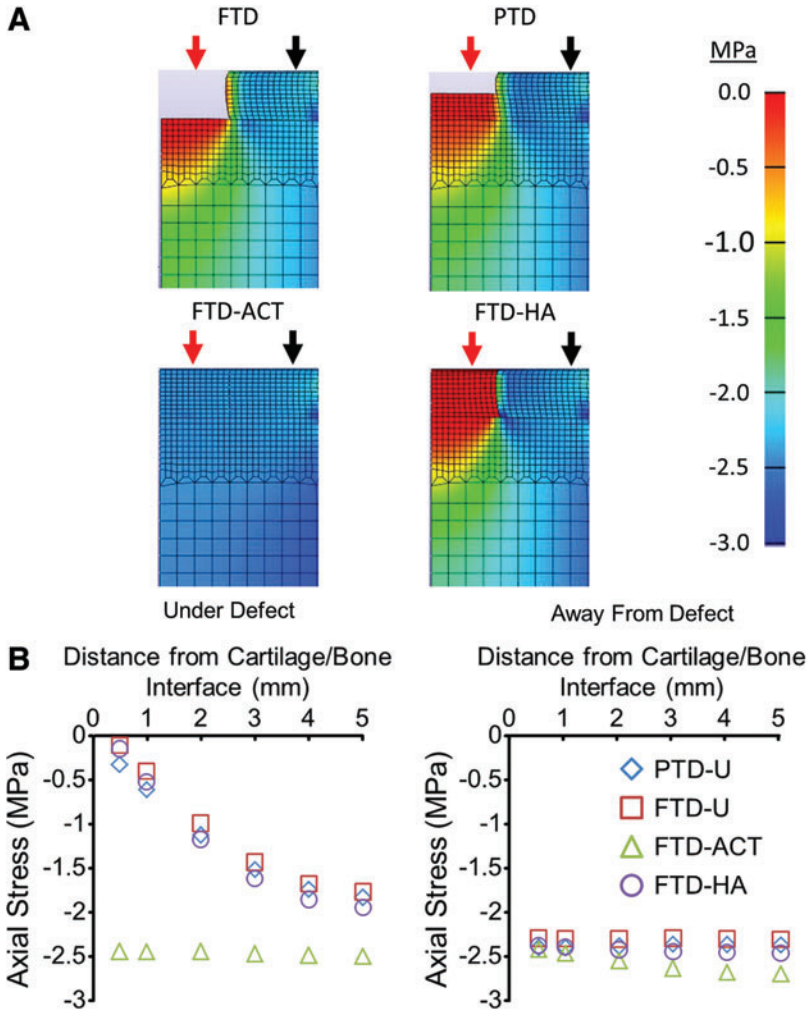

FIG. 8. Heat maps showing the axial stress in the defect, cartilage, and bone immediately after compression **(A)**. Stresses under (*red arrow*) and away from (*black arrow*) the defect for the various groups as a function of distance from the cartilage/bone interface **(B)**. Color images available online at www.liebertpub.com/tea

abnormalities observed here resolve toward the re-establishment of a patent subchondral architecture if provided a longer time course for healing and remodeling. In addition, the FE model utilized in this study could only predict the initial load transfer after treatment, but did not account for changes in implant properties, lateral integration to the host cartilage, or the more complex loading environment of the joint. More information regarding the mechanical properties of the tissue after treatment, healing, and remodeling are needed to determine whether the loads transmitted to the subchondral bone change during healing. Furthermore, the role of age in the development of such a response should be explored. In conclusion, the severity of a focal chondral defect dictates the amount of short-term bony remodeling in this immature porcine model. These data will guide future work in the evaluation of TE and regenerative medicine strategies for cartilage repair.

Acknowledgments

The authors thank Nicole Söegaard for her technical assistance. This work was supported by the National Institutes of Health (R01 EB008722 and F32 AR062971), the Department of Veterans Affairs (I01 RX000700), the AO Foundation, and the Orthopedic Research and Education Foundation (Resident Clinician Scientist Training Grant). The content is solely the responsibility of the authors and does not necessarily represent the official views of the National Institutes of Health or the Department of Veterans Affairs. No funding source had a role in the study design, collection, analysis and interpretation of data, writing of this article, or the decision to submit this article for publication.

Disclosure Statement

No competing financial interests exist.

References

1. Widuchowski, W., Widuchowski, J., and Trzaska, T. Articular cartilage defects: Study of 25,124 knee arthroscopies. Knee **14,** 177, 2007.
2. Curl, W.W., Krome, J., Gordon, E.S., Rushing, J., Smith, B.P., and Poehling, G.G. Cartilage injuries: a review of 31,516 knee arthroscopies. Arthroscopy **13,** 456, 1997.
3. Heir, S., Nerhus, T.K., Rotterud, J.H., Loken, S., Ekeland, A., Engebretsen, L., and Aroen, A. Focal cartilage defects in the knee impair quality of life as much as severe osteoarthritis: a comparison of knee injury and osteoarthritis outcome score in 4 patient categories scheduled for knee surgery. Am J Sports Med **38,** 231, 2010.
4. Guettler, J.H., Demetropoulos, C.K., Yang, K.H., and Jurist, K.A. Osteochondral defects in the human knee: influ-

ence of defect size on cartilage rim stress and load redistribution to surrounding cartilage. Am J Sports Med **32,** 1451, 2004.
5. Wang, Y., Ding, C., Wluka, A.E., Davis, S., Ebeling, P.R., Jones, G., and Cicuttini, F.M. Factors affecting progression of knee cartilage defects in normal subjects over 2 years. Rheumatology (Oxford) **45,** 79, 2006.
6. Brittberg, M. Cell carriers as the next generation of cell therapy for cartilage repair: a review of the matrix-induced autologous chondrocyte implantation procedure. Am J Sports Med **38,** 1259, 2010.
7. Alford, J.W., and Cole, B.J. Cartilage restoration, part 1: basic science, historical perspective, patient evaluation, and treatment options. Am J Sports Med **33,** 295, 2005.
8. Steadman, J.R., Rodkey, W.G., and Briggs, K.K. Microfracture to treat full-thickness chondral defects: surgical technique, rehabilitation, and outcomes. J Knee Surg **15,** 170, 2002.
9. Steadman, J.R., Rodkey, W.G., and Rodrigo, J.J. Microfracture: surgical technique and rehabilitation to treat chondral defects. Clin Orthop Relat Res **(391 Suppl),** S362, 2001.
10. Hangody, L., Kish, G., Karpati, Z., Szerb, I., and Udvarhelyi, I. Arthroscopic autogenous osteochondral mosaicplasty for the treatment of femoral condylar articular defects. A preliminary report. Knee Surg Sports Traumatol Arthrosc **5,** 262, 1997.
11. Baumbach, K., Petersen, J.P., Ueblacker, P., Schroder, J., Gopfert, C., Stork, A., Rueger, J.M., Amling, M., and Meenen, N.M. The fate of osteochondral grafts after autologous osteochondral transplantation: a one-year follow-up study in a minipig model. Arch Orthop Trauma Surg **128,** 1255, 2008.
12. Bartlett, W., Skinner, J.A., Gooding, C.R., Carrington, R.W., Flanagan, A.M., Briggs, T.W., and Bentley, G. Autologous chondrocyte implantation versus matrix-induced autologous chondrocyte implantation for osteochondral defects of the knee: a prospective, randomised study. J Bone Joint Surg Br **87,** 640, 2005.
13. Obradovic, B., Martin, I., Padera, R.F., Treppo, S., Freed, L.E., and Vunjak-Novakovic, G. Integration of engineered cartilage. J Orthop Res **19,** 1089, 2001.
14. Erickson, I.E., Kestle, S.R., Zellars, K.H., Farrell, M.J., Kim, M., Burdick, J.A., and Mauck, R.L. High mesenchymal stem cell seeding densities in hyaluronic acid hydrogels produce engineered cartilage with native tissue properties. Acta Biomater **8,** 3027, 2012.
15. Ng, K.W., O'Conor, C.J., Kugler, L.E., Cook, J.L., Ateshian, G.A., and Hung, C.T. Transient supplementation of anabolic growth factors rapidly stimulates matrix synthesis in engineered cartilage. Ann Biomed Eng **39,** 2491, 2011.
16. Cheng, N.C., Estes, B.T., Awad, H.A., and Guilak, F. Chondrogenic differentiation of adipose-derived adult stem cells by a porous scaffold derived from native articular cartilage extracellular matrix. Tissue Eng Part A **15,** 231, 2009.
17. Vinardell, T., Sheehy, E.J., Buckley, C.T., and Kelly, D.J. A comparison of the functionality and *in vivo* phenotypic stability of cartilaginous tissues engineered from different stem cell sources. Tissue Eng Part A **18,** 1161, 2012.
18. Lima, E.G., Bian, L., Ng, K.W., Mauck, R.L., Byers, B.A., Tuan, R.S., Ateshian, G.A., and Hung, C.T. The beneficial effect of delayed compressive loading on tissue-engineered cartilage constructs cultured with tgf-beta3. Osteoarthritis Cartilage **15,** 1025, 2007.
19. Erickson, I.E., Kestle, S.R., Zellars, K.H., Dodge, G.R., Burdick, J.A., and Mauck, R.L. Improved cartilage repair via *in vitro* pre-maturation of msc-seeded hyaluronic acid hydrogels. Biomed Mater **7,** 024110, 2012.
20. Burdick, J.A., Chung, C., Jia, X.Q., Randolph, M.A., and Langer, R. Controlled degradation and mechanical behavior of photopolymerized hyaluronic acid networks. Biomacromolecules **6,** 386, 2005.
21. Fisher, M.B., Henning, E.A., Soegaard, N.B., Dodge, G.R., Steinberg, D.R., and Mauck, R.L. Maximizing cartilage formation and integration via a trajectory-based tissue engineering approach. Biomaterials **35,** 2140, 2014.
22. Erickson, I.E., Huang, A.H., Chung, C., Li, R.T., Burdick, J.A., and Mauck, R.L. Differential maturation and structure-function relationships in mesenchymal stem cell- and chondrocyte-seeded hydrogels. Tissue Eng Part A **15,** 1041, 2009.
23. Chu, C.R., Szczodry, M. and Bruno, S. Animal models for cartilage regeneration and repair. Tissue Eng Part B Rev **16,** 105, 2010.
24. Ahern, B.J., Parvizi, J., Boston, R., and Schaer, T.P. Preclinical animal models in single site cartilage defect testing: a systematic review. Osteoarthritis Cartilage **17,** 705, 2009.
25. Chawla, K., Klein, T.J., Schumacher, B.L., Jadin, K.D., Shah, B.H., Nakagawa, K., Wong, V.W., Chen, A.C., Masuda, K., and Sah, R.L. Short-term retention of labeled chondrocyte subpopulations in stratified tissue-engineered cartilaginous constructs implanted *in vivo* in mini-pigs. Tissue Eng **13,** 1525, 2007.
26. Gotterbarm, T., Breusch, S.J., Schneider, U., and Jung, M. The minipig model for experimental chondral and osteochondral defect repair in tissue engineering: retrospective analysis of 180 defects. Lab Anim **42,** 71, 2008.
27. Dorotka, R., Windberger, U., Macfelda, K., Bindreiter, U., Toma, C., and Nehrer, S. Repair of articular cartilage defects treated by microfracture and a three-dimensional collagen matrix. Biomaterials **26,** 3617, 2005.
28. Frisbie, D.D., Oxford, J.T., Southwood, L., Trotter, G.W., Rodkey, W.G., Steadman, J.R., Goodnight, J.L., and McIlwraith, C.W. Early events in cartilage repair after subchondral bone microfracture. Clin Orthop Relat Res 215, 2003.
29. Lane, J.G., Healey, R.M., Chen, A.C., Sah, R.L., and Amiel, D. Can osteochondral grafting be augmented with microfracture in an extended-size lesion of articular cartilage? Am J Sports Med **38,** 1316, 2010.
30. Vasara, A.I., Hyttinen, M.M., Pulliainen, O., Lammi, M.J., Jurvelin, J.S., Peterson, L., Lindahl, A., Helminen, H.J., and Kiviranta, I. Immature porcine knee cartilage lesions show good healing with or without autologous chondrocyte transplantation. Osteoarthritis Cartilage **14,** 1066, 2006.
31. Li, W.J., Chiang, H., Kuo, T.F., Lee, H.S., Jiang, C.C., and Tuan, R.S. Evaluation of articular cartilage repair using biodegradable nanofibrous scaffolds in a swine model: a pilot study. J Tissue Eng Regen Med **3,** 1, 2009.
32. Liu, Y., Chen, F., Liu, W., Cui, L., Shang, Q., Xia, W., Wang, J., Cui, Y., Yang, G., Liu, D., Wu, J., Xu, R., Buonocore, S.D., and Cao, Y. Repairing large porcine full-thickness defects of articular cartilage using autologous chondrocyte-engineered cartilage. Tissue Eng **8,** 709, 2002.
33. Vasara, A.I., Hyttinen, M.M., Lammi, M.J., Lammi, P.E., Langsjo, T.K., Lindahl, A., Peterson, L., Kellomaki, M., Konttinen, Y.T., Helminen, H.J., and Kiviranta, I. Subchondral bone reaction associated with chondral defect and

attempted cartilage repair in goats. Calcif Tissue Int **74,** 107, 2004.
34. Orth, P., Goebel, L., Wolfram, U., Ong, M.F., Graber, S., Kohn, D., Cucchiarini, M., Ignatius, A., Pape, D., and Madry, H. Effect of subchondral drilling on the microarchitecture of subchondral bone: analysis in a large animal model at 6 months. Am J Sports Med **40,** 828, 2012.
35. Goulet, R.W., Goldstein, S.A., Ciarelli, M.J., Kuhn, J.L., Brown, M.B., and Feldkamp, L.A. The relationship between the structural and orthogonal compressive properties of trabecular bone. J Biomech **27,** 375, 1994.
36. Xie, L., Lin, A.S., Levenston, M.E., and Guldberg, R.E. Quantitative assessment of articular cartilage morphology via epic-microct. Osteoarthritis Cartilage **17,** 313, 2009.
37. Mainil-Varlet, P., Van Damme, B., Nesic, D., Knutsen, G., Kandel, R., and Roberts, S. A new histology scoring system for the assessment of the quality of human cartilage repair: ICRS II. Am J Sports Med **38,** 880, 2010.
38. Maas, S.A., Ellis, B.J., Ateshian, G.A., and Weiss, J.A. Febio: finite elements for biomechanics. J Biomech Eng **134,** 011005, 2012.
39. Ateshian, G.A., Rajan, V., Chahine, N.O., Canal, C.E., and Hung, C.T. Modeling the matrix of articular cartilage using a continuous fiber angular distribution predicts many observed phenomena. J Biomech Eng **131,** 061003, 2009.
40. Huang, C.Y., Soltz, M.A., Kopacz, M., Mow, V.C., and Ateshian, G.A. Experimental verification of the roles of intrinsic matrix viscoelasticity and tension-compression nonlinearity in the biphasic response of cartilage. J Biomech Eng **125,** 84, 2003.
41. Erickson, I.E., Huang, A.H., Sengupta, S., Kestle, S., Burdick, J.A., and Mauck, R.L. Macromer density influences mesenchymal stem cell chondrogenesis and maturation in photocrosslinked hyaluronic acid hydrogels. Osteoarthritis Cartilage **17,** 1639, 2009.
42. Pei, M., He, F., Li, J., Tidwell, J.E., Jones, A.C., and McDonough, E.B. Repair of large animal partial-thickness cartilage defects through intraarticular injection of matrix-rejuvenated synovium-derived stem cells. Tissue Eng Part A **19,** 1144, 2013.
43. Mainil-Varlet, P., Rieser, F., Grogan, S., Mueller, W., Saager, C., and Jakob, R.P. Articular cartilage repair using a tissue-engineered cartilage-like implant: an animal study. Osteoarthritis Cartilage **9 Suppl A,** S6, 2001.
44. Orth, P., Cucchiarini, M., Kohn, D., and Madry, H. Alterations of the subchondral bone in osteochondral repair—translational data and clinical evidence. Eur Cell Mater **25,** 299; discussion 314, 2013.
45. Chiang, H., Kuo, T.F., Tsai, C.C., Lin, M.C., She, B.R., Huang, Y.Y., Lee, H.S., Shieh, C.S., Chen, M.H., Ramshaw, J.A., Werkmeister, J.A., Tuan, R.S., and Jiang, C.C. Repair of porcine articular cartilage defect with autologous chondrocyte transplantation. J Orthop Res **23,** 584, 2005.
46. Pallante, A.L., Chen, A.C., Ball, S.T., Amiel, D., Masuda, K., Sah, R.L., and Bugbee, W.D. The *in vivo* performance of osteochondral allografts in the goat is diminished with extended storage and decreased cartilage cellularity. Am J Sports Med **40,** 1814, 2012.
47. Horas, U., Pelinkovic, D., Herr, G., Aigner, T., and Schnettler, R. Autologous chondrocyte implantation and osteochondral cylinder transplantation in cartilage repair of the knee joint. A prospective, comparative trial. J Bone Joint Surg Am **85-A,** 185, 2003.
48. Lane, J.G., Massie, J.B., Ball, S.T., Amiel, M.E., Chen, A.C., Bae, W.C., Sah, R.L., and Amiel, D. Follow-up of osteochondral plug transfers in a goat model: a 6-month study. Am J Sports Med **32,** 1440, 2004.
49. Mankin, H.J. The response of articular cartilage to mechanical injury. J Bone Joint Surg Am. **64,** 460, 1982.
50. Insall, J. The pridie debridement operation for osteoarthritis of the knee. Clin Orthop Relat Res 61, 1974.
51. Pallante-Kichura, A.L., Cory, E., Bugbee, W.D., and Sah, R.L. Bone cysts after osteochondral allograft repair of cartilage defects in goats suggest abnormal interaction between subchondral bone and overlying synovial joint tissues. Bone **57,** 259, 2013.
52. Hoemann, C.D., Hurtig, M., Rossomacha, E., Sun, J., Chevrier, A., Shive, M.S., and Buschmann, M.D. Chitosan-glycerol phosphate/blood implants improve hyaline cartilage repair in ovine microfracture defects. J Bone Joint Surg Am **87,** 2671, 2005.
53. Sharma, B., Fermanian, S., Gibson, M., Unterman, S., Herzka, D. A., Cascio, B., Coburn, J., Hui, A.Y., Marcus, N., Gold, G.E., and Elisseeff, J.H. Human cartilage repair with a photoreactive adhesive-hydrogel composite. Sci Transl Med **5,** 167ra166, 2013.
54. Bian, L., Zhai, D.Y., Tous, E., Rai, R., Mauck, R.L., and Burdick, J.A. Enhanced msc chondrogenesis following delivery of tgf-beta3 from alginate microspheres within hyaluronic acid hydrogels *in vitro* and *in vivo*. Biomaterials **32,** 6425, 2011.

Address correspondence to:
Robert L. Mauck, PhD
McKay Orthopaedic Research Laboratory
Department of Orthopaedic Surgery
Perelman School of Medicine
University of Pennsylvania
424 Stemmler Hall
36th St. and Hamilton Walk
Philadelphia, PA 19104

E-mail: lemauck@mail.med.upenn.edu

Received: June 28, 2014
Accepted: September 19, 2014
Online Publication Date: December 9, 2014